Journal Pre-proof

Sustained, Photocatalytic CO_2 Reduction to CH_4 in a Continuous Flow Reactor by Earth-Abundant Materials: Reduced Titania-Cu_2O Z-Scheme Heterostructures

Shahzad Ali, Junho Lee, Hwapyong Kim, Yunju Hwang, Abdul Razzaq, Jin-Woo Jung, Chang-Hee Cho, Su-Il In

PII: S0926-3373(20)30759-1

DOI: https://doi.org/10.1016/j.apcatb.2020.119344

Reference: APCATB 119344

To appear in: *Applied Catalysis B: Environmental*

Received Date: 19 May 2020

Revised Date: 4 July 2020

Accepted Date: 15 July 2020

Please cite this article as: Ali S, Lee J, Kim H, Hwang Y, Razzaq A, Jung J-Woo, Cho C-Hee, In S-Il, Sustained, Photocatalytic CO_2 Reduction to CH_4 in a Continuous Flow Reactor by Earth-Abundant Materials: Reduced Titania-Cu_2O Z-Scheme Heterostructures, *Applied Catalysis B: Environmental* (2020), doi: https://doi.org/10.1016/j.apcatb.2020.119344

Sustained, Photocatalytic CO_2 Reduction to CH_4 in a Continuous Flow Reactor by Earth-Abundant Materials: Reduced Titania-Cu_2O Z-Scheme Heterostructures

Shahzad Ali [a,b], Junho Lee [a], Hwapyong Kim [a], Yunju Hwang [a], Abdul Razzaq [b], Jin-Woo Jung [c], Chang-Hee Cho [c] and Su-Il In [a,d*]

[a] Department of Energy Science & Engineering, DGIST, 333 Techno Jungang daero, Hyeonpung-eup, Dalseong-gun, Daegu 42988, Republic of Korea

[b] Department of Chemical Engineering, COMSATS University Islamabad, Lahore Campus, 1.5 KM Defense Road, Off Raiwind Road, Lahore 54000, Pakistan

[c] Department of Emerging Materials Science, DGIST, 333 Techno Jungang daero, Hyeonpung-eup, Dalseong-gun, Daegu 42988, Republic of Korea

[d] Linde + Robinson Laboratories, California Institute of Technology, Pasadena, CA 91125, USA

*Email: insuil@dgist.ac.kr

Graphical Abstract

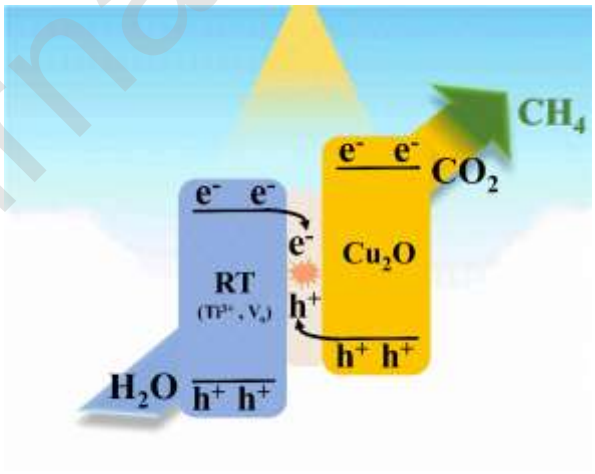

Highlights

- A stable and affordable Z-scheme heterostructure between reduced titania and Cu_2O with beneficial photocatalytic features is synthesized.
- The role of reduced titania in the formation of effective and stable geometrical configuration at the Z-scheme heterostructure interface is well explored.
- The effect of titania reduction degree over the performance of the Z-scheme heterostructure is studied.
- Dynamic charge transfer within the Z-scheme photocatalyst and its consequent effects over Cu_2O oxidation states are analysed in detail.
- The underlying mechanism for stable photocatalytic conversion of CO_2 and H_2O to CH_4 by the Z-scheme photocatalyst is elucidated.

Abstract

Photocatalytic conversion of CO_2 and water vapor to hydrocarbon fuels is a promising approach for storing solar energy while reducing greenhouse gas emissions. However, still certain issues including low product yields, limited photocatalyst stability and relatively high cost have hampered practical implementation of this technology. In the present work a unique strategy is adopted to synthesize a stable, and inexpensive photocatalyst comprised of earth-abundant materials: a reduced titania-Cu_2O Z-scheme heterostructure. Under illumination for 6 hours, the optimized reduced titania-Cu_2O photocatalyst enables 0.13% photoreduction of highly diluted CO_2 with water vapors to 462 nmol g^{-1} of CH_4 while showing excellent stability over seven testing cycles (42 h). Our studies show the Z-scheme inhibits Cu_2O photocorrosion, while its synergistic

effects with reduced titania result in sustained CH_4 formation in continuous flow photoreactor. To the best of our knowledge stability exhibited by the reduced titania-Cu_2O Z-scheme is the highest for any Cu-based photocatalyst.

Keywords

Reduced titania; Oxygen vacancy; Photocatalysis; Z-scheme heterostructure; Copper oxide.

Abbreviations

RT, Reduced titania; V_o, Oxygen Vacancies; IFCT, interfacial charge transfer.

1. Introduction

Unwanted climate change is driving a global shift towards renewable energy sources [1,2]. Solar-driven conversion of CO_2 to fuel, particularly a fuel compatible with the current energy infrastructure, is a technology promising in its potential ability to resolve the interlinked issues of satisfying energy demand while minimizing deleterious environmental impacts [3,4]. Photocatalytic CO_2 reduction, relative to its peers i.e. thermo-catalytic, can enable a thermodynamic uphill reaction to occur even under ambient, non-concentrated sunlight [5]. However while such a technology is immensely intriguing, and desirable, offering the ability to store and transport solar energy in the form of liquid or gas-phase fuel, a commercially enabling photocatalyst (low cost, stable, highly-efficient, etc.) has yet to be achieved [6] due to inherent limitations with the photocatalyst such as rapid (unwanted) charge recombination, limited solar spectrum response, and stability [3,7,8]. It is well established that reduced titania (RT), due to the inherent defect states (Ti^{3+} states and oxygen vacancies V_o), along with the use of metal co-

catalysts may substantially overcome such limitations to viably convert CO_2 to useful chemicals/fuels [9,10]. However literature indicates that precise control of defect state density is critical to achieving a high performance photocatalyst [11], and difficult to do without high temperature reduction processes [12]. Further, combining RT with noble metal based co-catalysts notable for promoting photocatalyst activity, e.g. Pt, Au, Ag, Rh, and Pd, results in a relatively expensive photocatalyst [13,14] not amenable to large scale implementation. However this concern can be allayed by the fabrication of photocatalyst comprised of RT, synthesized under mild conditions, with non-noble metals i.e. copper oxides CuO/Cu_2O [15,16] active in response to visible-spectrum illumination.

The behavior of Cu/CuO/Cu_2O based photocatalysts is well documented in the literatures [16,17]. For photocatalytic CO_2 reduction the most agreeable oxidation state (+1) is possessed by Cu_2O [18]. With a band gap of ~2.0-2.2 eV and highly energetic conduction band (i.e. -1.27 eV), Cu_2O suffers from photocorrosion owing to the limited water oxidation capability of its holes; holes accumulate on the material surface and there oxidize Cu_2O since its oxidation potential lies within its band gap [16,19]. However, stability can be maintained by the formation of a TiO_2-Cu_2O direct Z-scheme heterostructure. Upon illumination, electrons from the TiO_2 conduction band (CB) scavenge holes from Cu_2O while preserving the strongly reductive electrons on the CB of Cu_2O [20–22]. Similarly, strong oxidative holes present at the TiO_2 valence band (VB) are also preserved, and a spatial charge separation is achieved across the TiO_2-Cu_2O interface. Such charge separation, achieved by virtue of neutralizing the holes from Cu_2O, assures the sustained supply of these preserved photo-generated charges (e^-/h^+) for photocatalytic CO_2 reduction [23].

It has been admitted that geometrical configurations by which both photocatalysts of the Z-scheme are attached to each other play a pivotal role in determining the activity [24]. Generally, a large

interfacial contact for such structures is highly desirable to garner more benefits [25]. To date various Cu based Z-scheme heterostructure symmetries have been fabricated which include; (i) surface deposited heterostructures, (ii) core-shell heterostructures and (iii) Janus-like systems [21,25,26]. Surface decorated systems despite their beneficial properties may corrode owing to exposure of interface to ambient environment which can be avoided by developing core-shell structure. In the core-shell structure, shell protects the core and interface from corrosion, however in such arrangement electrons/holes accumulated on masked core are unable to participate in photocatalytic reaction directly [27]. For curbing such constraints a configuration, which is capable of abating corrosion of the interface, with exposed surfaces of the both catalysts may surely prove conducive, interestingly Janus-like structure has the former feature but possessing later one is challenging for them [25].

To the best of our knowledge few studies exist related to synthesis of ZnO-Cu_2O heterostructure with exposed photocatalyst surfaces however, they lack insights into maintaining the stability [28,29]. Motivated from this, herein we synthesize, characterize, and test a Z-scheme heterostructured photocatalyst of reduced titania and Cu_2O, abbreviated as RT-Cu_2O, by a unique synthesis approach. We envision the disorder shell present over the periphery of RT paves the way for the formation well defined RT-Cu_2O interface. The synthesis strategy is based upon a low temperature thermochemical reduction of TiO_2 followed by photo-deposition of Cu_2O nanoparticles. The simple synthesis steps intrinsic to the RT-Cu_2O Z-scheme heterostructure, which employ moderate reduction conditions for titania and relatively inexpensive precursors, result in relatively cost-affordable photocatalyst that demonstrates excellent sustained operational stability.

2. Experimental

2.1. Materials and preparation methods

2.1.1. Synthesis of reduced titania nanoparticles

Optimally reduced titania nanoparticles, named as RT, were synthesized by adopting a previously reported procedure [11]. In brief, P25 (200 mg) and $NaBH_4$ (98%), procured from Degussa and Alfa Aesar respectively, were shear mixed using a mortar and pestle. The resultant mixture was reduced under Argon atmosphere in quartz tube furnace at 350 °C for 30 minutes. The reduced mixture was then washed five times with an ample amount of deionized (DI) water and ethanol, followed by drying of washed RT nanoparticles in vacuum oven at 90 °C for 12 h. In similar fashion, slightly reduced (RT_s) and highly reduced titania (RT_h), by adding 20 and 40 mg of $NaBH_4$ respectively, were prepared and their photocatalytic performance was evaluated against the optimized RT sample.

2.1.2. Synthesis of Cu decorated RT nanoparticles

The as-prepared RT nanoparticles (100 mg) were mixed in different volumes (ml) of $CuSO_4 \cdot 5H_2O$ (Alfa Aesar 99%) standard solution (concentration of 1 mg/ml) following the method of [9]. Later, 5 ml of methanol and makeup DI water were added to above mixture to make a final volume of 25 ml. After mixing for 1 h under dark, the suspension was irradiated for 2 h by a 300 W Xe lamp (Newport), 1 Sun condition, resulting in photo-deposition of Cu upon the RT. A schematic drawing of the synthesis procedure is shown in Fig. S1. The final product was washed with DI water and dried under vacuum at 90 °C for 12 h. A number of samples were prepared in which the Cu content varied, using different volumes of the $CuSO_4 \cdot 5H_2O$ standard solution. The resultant samples were designated as RT-Cu_x, (where x represents the weight percentage of the Cu

for various values of x = 0.25, 0.50, 0.60, 0.75, 0.90 and 1.00 wt.%). The term RT-Cu_x is utilized for representing effect of amount of Cu loading on various photocatalytic properties, while RT-Cu_2O is a general terminology representing the Z-scheme formed among RT and Cu_2O after Cu loading. Following the described procedure, the control samples P25- $Cu_{0.75}$, RT_s- $Cu_{0.75}$ and RT_h-$Cu_{0.75}$, were also synthesized. Cu_2O (Sigma Aldrich, 99%) was utilized as a standard for characterization with RT-Cu_2O.

2.2. Characterization methods

X-ray diffraction patterns were acquired using a PANalytical, Empyrean X-ray diffractometer with Cu kα radiation (λ = 1.54 Å) working at applied voltage and current of 40 kV and 30 mA, respectively. Elemental mapping and lattice fringe dimensions were recorded by field emission transmission electron microscopy (FE-TEM), Hitachi HF-3300 at 300 kV. Light absorption properties, in the range of λ = 200-800 nm, were determined by a Cary series UV-visible near infrared spectrophotometer equipped with an integrating sphere accessory providing UV-visible diffuse reflectance spectra (UV-vis DRS). Photoluminescence (PL) spectroscopy was performed with a Cary Eclipse fluorescence spectrophotometer (excitation λ = 320 nm). The Ti 2p, O 1s, and Cu 2p spectra were recorded using a Thermo VG, K-alpha using Al Kα line as the X-ray source in X-ray photoelectron spectroscopy (XPS). A Jeol-FA100 spectrometer was used at 100 K for recording the electron paramagnetic resonance (EPR) spectrum. Fourier-transform infrared (FTIR) analysis of pressed powder samples prepared in KBr was performed using a Thermo Scientific Nicolet Continuum spectrometer. Time-resolved PL measurements were performed using a home-built optical microscope system at room-temperature. The sample was excited by a pico-second pulsed diode laser (PicoQuant, LDH-P-FA-355) with a 355 nm wavelength (FWHM = 56 ps) and

repetition rate of 40 MHz. The excitation source was focused from 40× (NA = 0.6) objective (Nikon).

2.3. Photocatalytic testing

The experiments for photocatalytic CO_2 reduction in the presence of water vapor were performed under ambient conditions in a flow photoreactor, shown in Fig. 1 [30]. Briefly, 40 mg of photocatalyst was uniformly distributed over a porous ceramic disc placed inside a gas tight stainless steel photoreactor equipped with manually controlled gas inlet and outlet valves. Gas flow, controlled by a mass flow controller, was passed through a water bubbler for saturation resulting in 'moist' CO_2. Prior to each experiment the photoreactor was preconditioned three times with purging and evacuation (6.5×10^{-3} torr) by moist CO_2, at a flow rate of 40 ml/min. After purging the flow rate was adjusted to 1.0 ml/min, and the photocatalytic CO_2 experiment was carried out under simulated solar light illumination (1 Sun), provided by100 W solar simulator (Oriel, LCS-100) with an AM 1.5 filter. Photoreactions were monitored by an online gas chromatograph (Shimadzu, GC-2014, Restek-Rt-Q-bond column, length = 30 m and ID = 0.53 mm) with a flame ionization detector (FID) and He carrier gas. While for H_2 detection molecular sieve column (5A, G3591-7003 2 m x 1/8 inch, 2 mm SS packed) with Ar as carrier gas was used in Agilent (7890B) GC. The GC was programmed to analyze products from the photoreactor through an automated gas sampling valve every 0.5 h. Each catalyst was tested for 6 h, then regenerated through vacuum annealing at 100 °C for 2 h in accord with previous reports [9]. The stability of the optimized photocatalyst was determined by performing repeated CO_2 photoreduction experiments after regeneration.

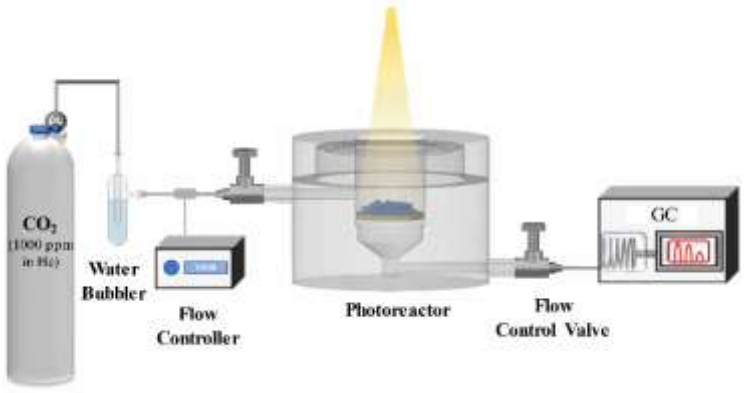

Fig. 1 Schematic illustration of the experimental setup for photocatalytic CO_2 reduction.

An isotopic labeling experiment was performed with $^{13}CO_2$ (Aldrich, ^{13}C 99% and 1000 ppm in He) to fix the carbon source responsible for hydrocarbon generation. The resultant $^{13}CH_4$ was identified by GC-MS (Shimadzu, GC–MS-QP2010 ultra; Restek-Rt-Q-bond column, length = 30 m and ID = 0.32 mm). Three other control experiments were performed to confirm the validity of our results, one without the presence of a photocatalyst and second under dark and last one after replacing the feed gas mixture (1000 ppm $^{12}CO_2$ in He) with pure He. Identical conditions for testing and analysis were constantly maintained except for the isotopic, CO and H_2 detection experiments conducted in a batch reactor with products analyzed at 1 h increments.

3. Results and Discussions

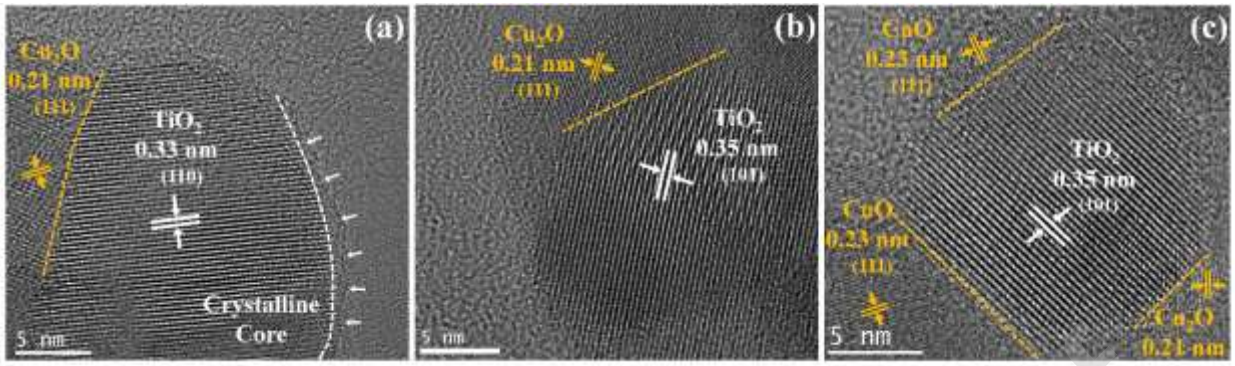

Fig. 2. (a-c) HR-TEM images of a RT-$Cu_{0.75}$ sample in which the inter-planar spacing of TiO_2, Cu_2O and CuO are observed.

X-ray diffraction (XRD) patterns obtained for P25, RT and various RT-Cu_x samples are shown in Fig. S2. It is obvious that no significant change appears in the TiO_2 crystalline phases with all samples displaying prominent peaks of both anatase and rutile phases, being thus composed of mixed crystalline phase after thermochemical reduction and Cu photo-deposition [31]. The XRD peaks corresponding to Cu are not observable, presumably due to their low concentration [32]. However, the presence of Cu is confirmed by employing TEM-based elemental mapping, Fig. S3. The high resolution transmission electron microscopy (HR-TEM) images for a representative RT-$Cu_{0.75}$ sample, Fig. 2(a-c), exhibits a clear depiction of lattice fringes with inter-planar spacing of 0.35 nm and 0.33 nm, which are ascribed to the (101) and (110) planes of anatase and rutile TiO_2, respectively [33]. The outer shell of the crystalline TiO_2 (Fig. 2a) looks to be amorphous as pointed by white arrows, which is attributed to the defects induced by the reduction process [11]. Such phase disordering within the shell region is further supported by Raman shift towards a higher wavenumber as well as peak broadening of the RT sample, shown in the inset of Fig. S4 [34]. The lattice spacing of 0.21 nm and 0.23 nm (Fig. 2c) correspond to the Cu_2O (101) and CuO (111) planes, respectively [35,36]. These copper oxides form an apparent and

distinguishable interfacial contact with the TiO_2, as indicated by the dashed yellow lines, after which it is challenging to detect the defected shell [29]. This interface is formed along the circumference of the crystalline core where trapped photogenerated electrons in the shell attract and then reduce the Cu ions during photodeposition process [25]. As a result, formed interface at the shell resists its oxidation due to enriched electron density and also, it endows crystalline core to exhibit its optical and catalytic features. We envisage these remarkable features may give it the potential to fix the challenges faced by different geometrical arrangements.

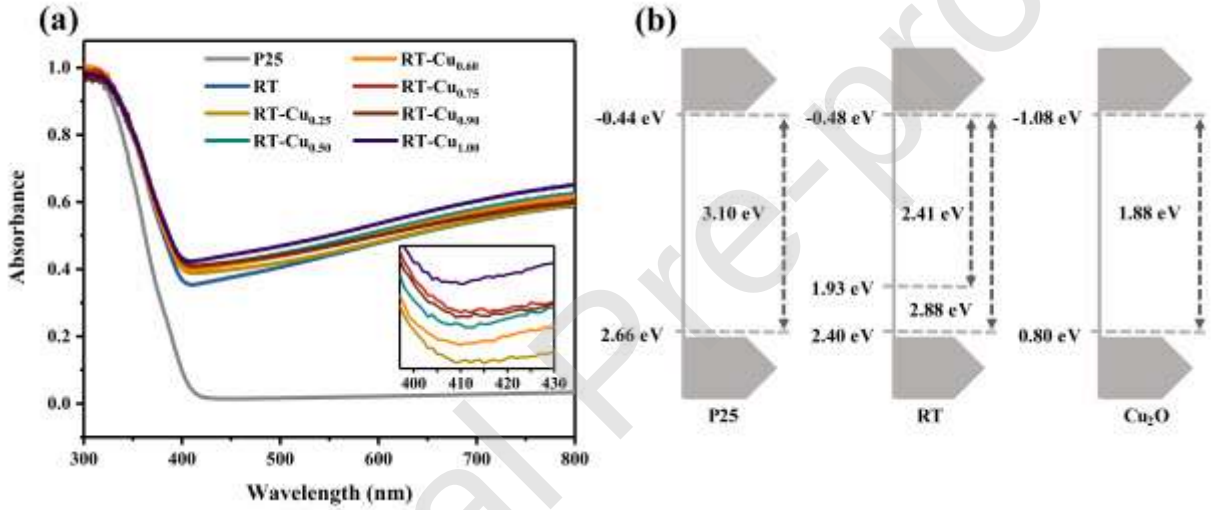

Fig. 3. (a) UV-vis DRS spectra for P25, RT, and various RT-Cu_x samples, and (b) energy band diagrams for P25, RT and Cu_2O.

Fig. 3a shows the UV–vis diffuse reflectance spectra of P25, RT, and various RT-Cu_x samples. As compared to P25, RT samples exhibit a red shift in absorbance with a significant increase in absorption intensity in the visible range. This red shift is attributed to defect formation in the RT, with the generated mid-gap states narrowing the band gap [31,34]. Upon Cu deposition the optical absorbance is further extended (inset Fig. 3a), specifically in the range λ = 400-500 nm, which can be ascribed to interfacial charge transfer (IFCT) from VB of RT to Cu_2O/CuO [37].

However, among the Cu deposited RT samples the absorption edge did not change significantly. Such type of trend is often observed when small amount of Cu is deposited on TiO_2 edges to form the clear interface. This trend is remarkably different from Cu doped samples where absorption edge shifts to higher wavelengths significantly [38]. This type of clear interface IFCT is perhaps most easily understood by combining the results obtained from the Tauc's plot (Fig. S5a) and VB-XPS results (Fig. S5(b-d)) to sketch the energy band diagrams shown in Fig. 3b [34]. The resultant band alignment suggests the heterostructure formation at the RT-Cu_2O interface which ultimately facilitates the rapid charge transport.

Fig. S6a shows the XPS survey scan for a representative RT-$Cu_{0.75}$ sample, revealing the presence of Ti, O, and Cu. The actual elemental composition of the Cu for this sample, determined from the XPS is 0.64% which corroborates the presence of majority Cu on the surface. Literatures suggest that an equilibrium is always established between Cu deposited and present in precursor solution during photodeposition process under specific set of conditions. However, interplay of these conditions, i.e. irradiated light intensity, photodeposition time, precursors ($CuSO_4 \cdot 5H_2O$) and hole scavenger concentration, can assist to extend the Cu loadings [39]. XPS spectra of Ti 2p and O 1s for P25 and RT, shown respectively in Fig. 4a and Fig. S6b, generally exhibit identical peak shapes except for a slight shift towards lower binding energies for RT. Such a shift in binding energy is always observed when electrons are transferred from reducing agent to oxygen of TiO_2 for creating V_o and then these provided electrons at V_o are transferred to Ti^{4+} for generating Ti^{3+} states [40,41]. The Cu 2p XPS spectra for RT-$Cu_{0.75}$ (Fig. 4b) display two peaks appearing at binding energies of 932 eV and 951.8 eV corresponding to Cu $2p_{3/2}$ and Cu $2p_{1/2}$ respectively; these binding energies are commonly attributed to the presence of Cu^{1+} [42]. The signatory satellite peak for Cu^{2+}, which appears in the region of 940-945 eV, is not observed in the XPS spectra [43], a result

in accordance with prior studies wherein this oxidation state is often undetected in XPS analysis despite the presence of Cu^{2+} [26,44]. XPS analysis for tested RT-$Cu_{0.75}$ (6 cycle), as shown in Fig. 4c, reveals a further shift towards lower binding energy, which suggests reduction of Cu^{2+} to Cu^{1+} and ultimately Cu^0 by electron injection from RT [45–47].

Charge transfer across RT-Cu_2O interface is further confirmed by the difference in EPR spectra of fresh and tested (1 cycle) RT-$Cu_{0.75}$, Fig. 4d. The EPR signal appearing at g = 1.99 indicates the occurrence of Ti^{3+} states while signals at g = 2.1 corresponds to traces of EPR active Cu^{2+} [26]. Such presence of Cu^{2+} is often detected in combination with Cu^{1+} while synthesizing Cu_2O [26,44]. It can be conceptualized herein that the relative ratio of Cu^{2+}/Cu^{1+} oxidations states depends upon the ability of RT to provide photogenerated electrons for reducing Cu^{2+} ions during photodeposition process. We believe an optimally reduced titania can guarantee the propitious number of electrons for reduction [48]. However, it could be speculated that when certain amount of the Cu is deposited the diffusion pathway for electrons increases. In this scenario, a smaller number of electrons reach the surface for Cu reduction leading to an increase in deposition of the Cu^{2+} [26]. After photocatalytic testing the Cu^{2+} signal intensity decreased, which indicates gradual transformation, under light illumination, of EPR active Cu^{2+} to Cu^{1+}/Cu^0 caused by electrons from RT [49]. Another, possible reason to help avert oxidation of the Cu can be the continuous removal of the produced oxygen owing to the flow photoreactor. However, a portion of that oxygen is not capable to desorb from the photocatalyst because CO_2 dissociated over V_o partially heals it, consequently sharpness of Ti^{3+} labelling signal for tested sample is decreased [5,50].

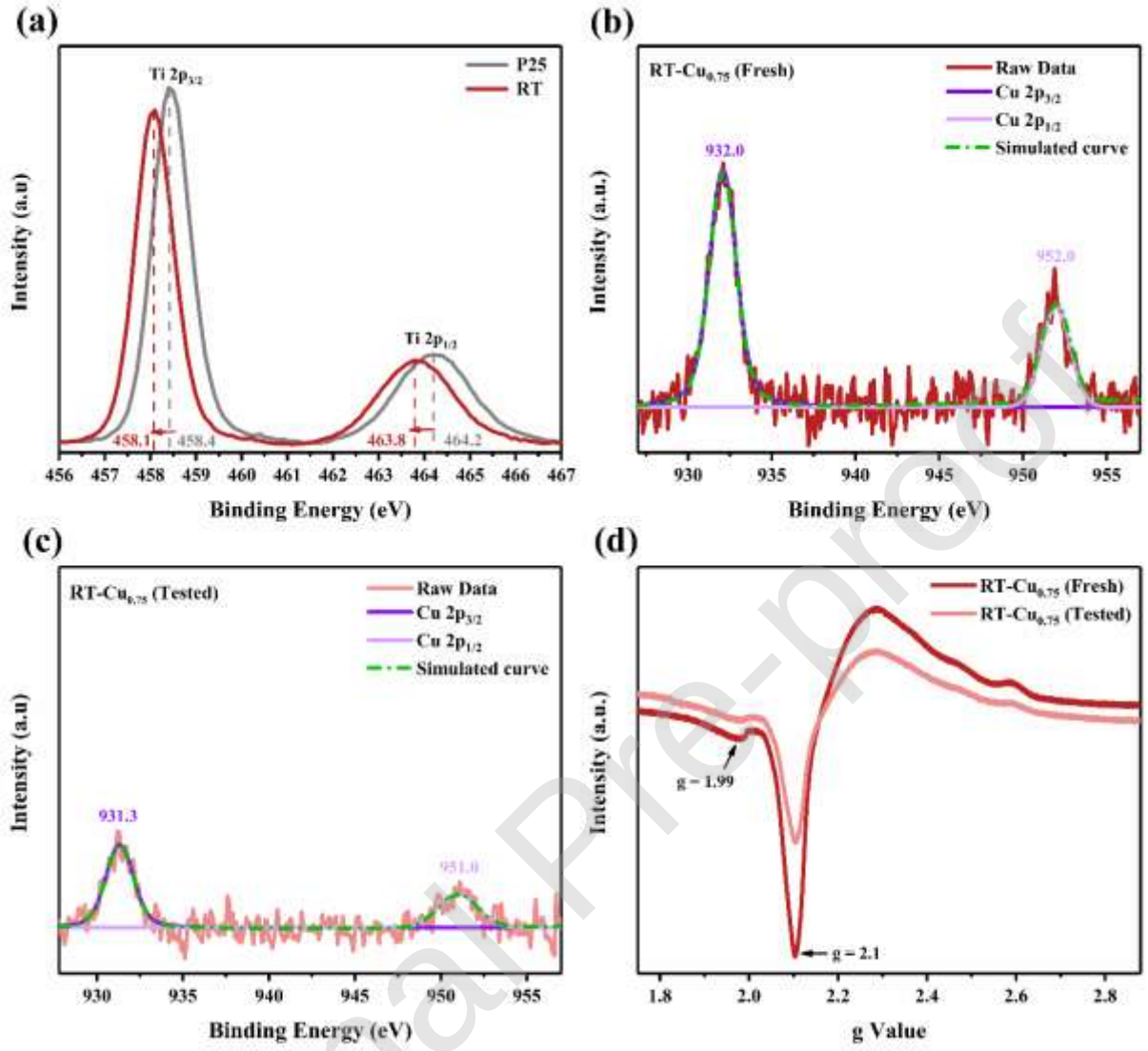

Fig. 4. (a) Ti 2p XPS spectra for P25 and RT samples; Cu 2p spectra for (b) fresh RT-$Cu_{0.75}$ and (c) tested RT-$Cu_{0.75}$; (d) EPR spectra of fresh and tested RT-$Cu_{0.75}$ samples.

A coumarin dye test, the details of which are provided in the supplementary text, was performed to further understand charge separation across the RT-Cu_2O interface and type of heterostructure formed [51]. In this test charge separation is directly related to the concentration of luminescent 7-hydroxycoumarin. As shown in Fig. S7, RT-$Cu_{0.75}$ exhibits higher fluorescence intensity indicating abundant photocatalytic generation of hydroxyl radicals (•OH), which

ultimately reacts with coumarin to produce more 7-hydroxycoumarin (Coumarin + •OH → 7-hydroxycoumarin). Cu_2O is incapable of responding to a coumarin dye test as its VB edge, evidenced from VB-XPS results (Fig. S5a), lies above the required oxidation potential (2.3 eV vs NHE) for OH^-/•OH transformation [51,52]. The enhanced oxidation capability of holes achieved with the optimized RT-Cu_2O, and so too the electron transfer from RT to Cu_2O, unequivocally endorse the Z-scheme charge transfer mechanism at the RT-Cu_2O interface.

PL studies provide a valuable information for studying charge transport and their separation across such heterostructures. PL spectra, Fig. 5a, indicate decreased intensity for RT in comparison to P25 which is attributed to mid-gap state localization of electrons which, in turn, ultimately favors their separation [53,54]. Further, the PL intensity decreased significantly for the RT-$Cu_{0.75}$ sample indicating effective charge separation and transport across the RT-Cu_2O interface [55]. To gain further insight time resolved PL was performed and the acquired decay traces were bi-exponentially fitted, Fig. 5b, using Eq. S1 based on decay times ($\boldsymbol{\tau}$) and their amplitudes (A) [56]. The average emission life time ($\boldsymbol{\tau_{avg}}$), is generally a combination of fast decay component ($\boldsymbol{\tau_1}$) and slow decay component ($\boldsymbol{\tau_2}$), was calculated from Eq. S2 and summarized in Table S1 [57]. The average life time for P25, RT and RT-$Cu_{0.75}$ decreased respectively which is consistent with trends of steady state PL emissions. The reduced life time for RT compared to P25 can be attributed to capturing of photogenerated charges by V_0 and shortest life time for RT-$Cu_{0.75}$ is interlinked with spatial charge separation across the Z-scheme RT-Cu_2O interface [58]. This spatial charge separation which prolongs recombination of electrons and holes is achieved on account of Z-scheme charge transfer mechanism [23].

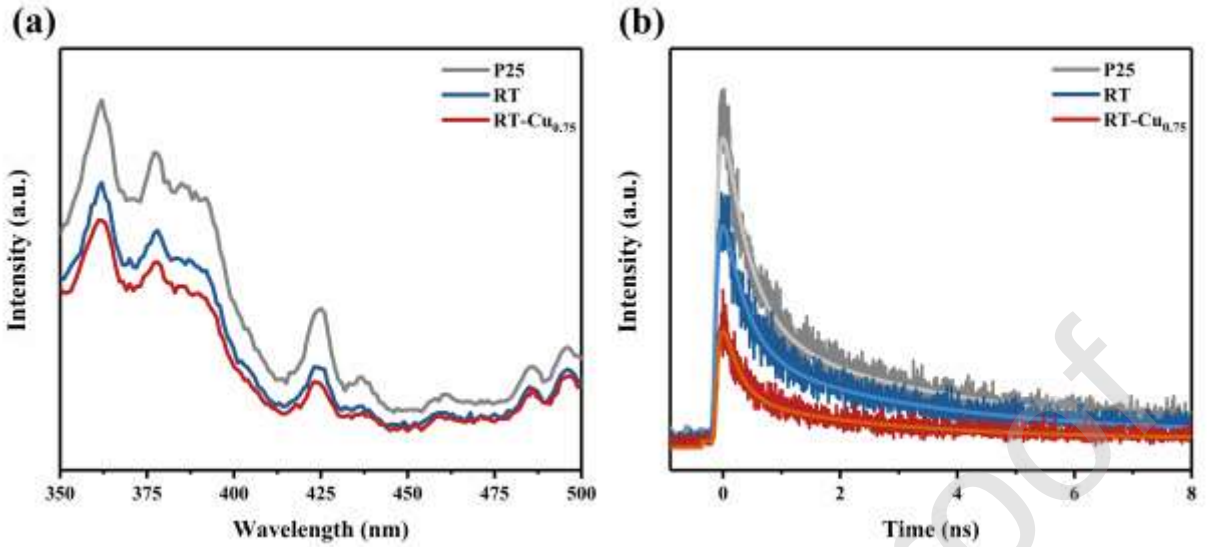

Fig. 5. (a) PL; (b) and time resolved PL curves for P25, RT and RT-$Cu_{0.75}$ samples.

Photocatalytic reduction tests for P25, RT, and RT-Cu_x samples found CH_4 as the primary product with trivial amounts of other products like C_2H_4, and C_2H_6. The CH_4 production rate for a 6 h test is shown in Fig. 6a and summarized in Table S2. It can be seen that P25 exhibited negligible photocatalytic activity, but showed improved CH_4 yield after reduction to RT. CH_4 yield was found to increase for the RT-Cu_x samples up to an optimum Cu concentration of 0.75 wt.% (RT-$Cu_{0.75}$), after that it showed a decline in performance. That optimized sample, RT-$Cu_{0.75}$, showed an accumulative yield of 462 nmol g^{-1} in 6 h at a rate of 77 nmol g^{-1} h^{-1} which is 10 times higher than RT. Such trends in photocatalytic performance are obtained when ideal charge separation is obtained by formation of an optimum interface between RT and Cu_2O [23]. A five-fold enhancement in CH_4 yield is observed for the optimized sample as compared to control sample P25-$Cu_{0.75}$ (Fig. S8). This enhanced photocatalytic activity lies in effectiveness of V_o in RT to capture the photogenerated electrons than P25 which lacks this feature [11]. Further, synergistic effects of Cu^{1+} and RT that have been proven efficacious for expedient destabilization and reduction of CO_2 to spur the activity [5]. These effects are further pronounced by the beneficial

attributes of a Z-scheme heterostructure: better charge separation, strong reductive electrons and oxidative holes [23,59]. Another, possible reason for the improvement in stability can be attributed to the continuous flow reaction mode [30]. Usually, in gas phase photo-reactions under-stoichiometric oxygen, a byproduct of photocatalytic CO_2 reduction, is observed which is possibly due to its adsorption over the photocatalyst [60]. The removal of the oxygen from the reaction medium is essential because other than healing V_o the molecular oxygen competes with CO_2 for electron intake [32]. Thus, flow reaction mode attempts to relieve the gaseous products uninterruptedly by which yield is improved. A separate study is needed to understand the in-depth mechanism by which presence of oxygen hampers the activity of the photocatalyst.

To evaluate the relative effect of defect sites induced by reduction of TiO_2, the CH_4 yield obtained for RT-$Cu_{0.75}$ was compared with slightly reduced TiO_2 (RT_s-$Cu_{0.75}$) and highly reduced TiO_2 (RT_h-$Cu_{0.75}$) having similar Cu deposition. The CH_4 yields obtained for the mentioned samples are shown in Fig. 6b. It can be observed that both the samples i.e. RT_s-$Cu_{0.75}$ and RT_h-$Cu_{0.75}$ exhibit lower CH_4 yields as compared to the optimized sample, RT-$Cu_{0.75}$, hence corroborating the effect of defected sites induced by reduction process to be a significant aspect of photocatalytic performance. Limited defects are not conducive enough to change the bandgap appreciably which may eventually reflect in double faceted effect; as not only limited photogenerated charges will curtail the Cu deposition but also the photocatalytic performance will descend when such under optimized interface will be illuminated [11]. Interestingly, large density of defects reduces the bandgap appreciably, but in turn over-optimized defected states also serve in fast recombination of the photogenerated charges. However, during Cu photodeposition, higher flux of electrons and holes can be readily accepted by Cu^{2+} ions and methanol respectively, by which presumably excess amount of Cu is deposited. As discussed already, with the propagation

of Cu thickness, inactive oxidation state (Cu^{2+}) starts dominating [61]. Furthermore, the efficacy of the defected sites can be explained on the account of charge generation, and separation among variable defected states, and formation of RT-Cu_2O interface. In summation, a tradeoff should be considered in degree of reduction and exhibited optical properties to achieve better yields. Thus, optimally reduced titania resulted in the formation of well-defined interface with desirable oxidation states which have led to better performance. Apparently, it seems our tested photocatalysts are producing yield in nanomoles, but in terms of CO_2 conversion, our optimized sample enabled 0.13% conversion of the highly diluted feed gas (1000 ppm CO_2 in He). Despite of using highly diluted feed gas, this performance seems exceptional and we believe this could be enhanced while optimizing the dilution/concentration of the CO_2 with improvement in other operating parameters like pressure, temperature etc. [30].

In addition to better performance, the RT-$Cu_{0.75}$ samples showed excellent stability over the course of seven testing cycles, see Fig. 7a. After each 6 h cycle the photocatalyst was vacuum annealed at 100°C for 2 h, an un-optimized temperature and anneal duration. Vacuum annealing revamps the activity of almost dormant photocatalyst, presumably by regenerating V_o which have been cured during photoreduction by O atom of CO_2 or decomposing and desorbing the formed intermediates which are harbored at active sites and difficult to decompose by the photocatalytic action [5,9]. These decomposed intermediates are further converted to a vulnerable form for photo-reduction which eventually superimpose the yield from CO_2 reduction, as evident from 3rd and 6th run. Also, some formed intermediates, like formates, serve as hole scavengers thereby improved electron availability adds to higher yield [62]. We noted such a vacuum anneal step could be readily implemented, if or as needed, within a computer-controlled system removing the need for physical handling of the photocatalyst.

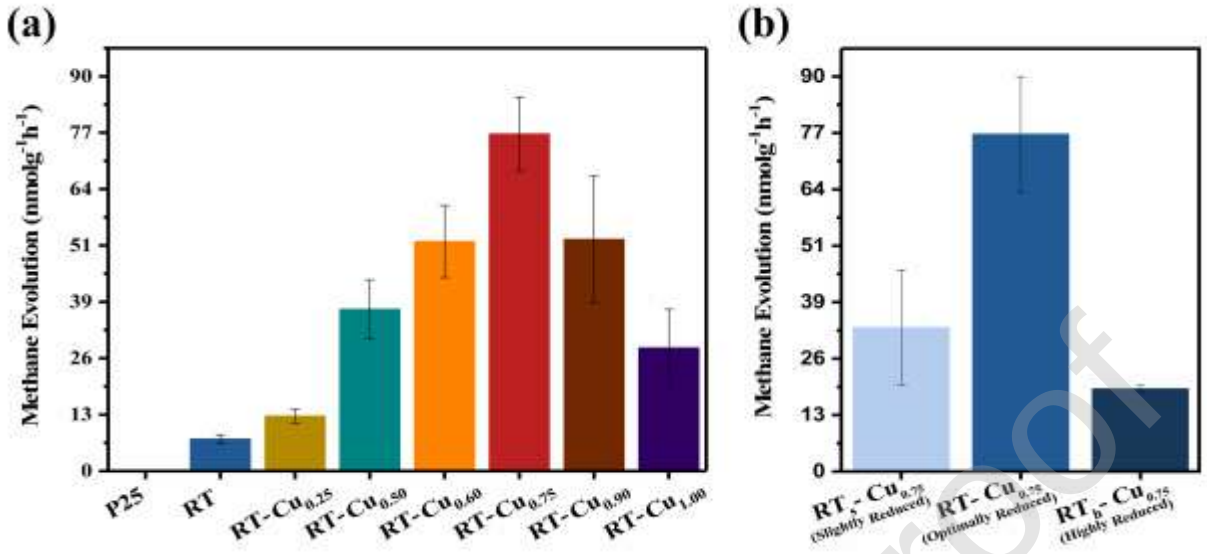

Fig. 6. (a) Comparison of CH_4 evolution over a 6 h test for P25, RT, and RT-Cu_x; (b) CH_4 evolution for variable reduction degree from slightly reduced RT_s-$Cu_{0.75}$ to highly reduced RT_h-$Cu_{0.75}$.

We believe the excellent stability is due to the direct Z-scheme charge transfer mechanism across well designed interface which inhibits Cu_2O photocorrosion. Here, in contrast to earlier reports pertinent to heterostructure interfaces, upon illumination photogenerated electrons from the CB of RT are trapped at V_o in defected shell. This electron-enriched shell stimulates the quenching of the Cu_2O VB holes at the interface which are responsible for its photocorrosion [21,22], yet still ineffective for water oxidation due to their lower oxidation potential. Thus, with elimination of the 'weaker' electrons and holes their 'stronger' reductive/oxidative counterparts are preserved, as illustrated in Fig. 7b [23,59]. The large over-potential available for photocatalytic CO_2 reduction translates into an actual quantum yield (A.Q.Y) of 0.012 and joule sunlight to joule fuel efficiency of 1.4 x 10^{-4} as shown in Table. S2 [63,64]. As can be seen from Table S3, performance stability we achieve with our sample, in application to gas phase photocatalytic CO_2 reduction with H_2O, is the highest reported. After 7 cycles, the photocatalyst lost the stability in performance and a sharp decline was observed in CH_4 production. The stability loss may be

attributed to change in the oxidation state of the $Cu^{2+/}Cu^{1+}$ to Cu^0 after photocatalytic reaction, as supported by post reaction XPS. Thus, upon repeated irradiations Cu^{1+}, active oxidation state for photocatalytic CO_2 reduction as noticed by several studies, gradually reduces to Cu^0 with intermediate oxidation state of $Cu^{1+/}Cu^0$ [32,49,55]. This intermediate oxidation state is even also conducive for photocatalytic CO_2 reduction, where Cu^0 can capture photogenerated electrons, by the virtue of low Fermi level, and Cu^{1+} being desirous active state can promote CH_4 formation [55,65]. The Cu^{2+} reduction is presumably due to presence of excessive numbers of electron than the stochiometric amount to quench the holes. Finally, when all the Cu^{1+} reduces to Cu^0, the Z-scheme no longer exists which eventually concludes in the stability loss.

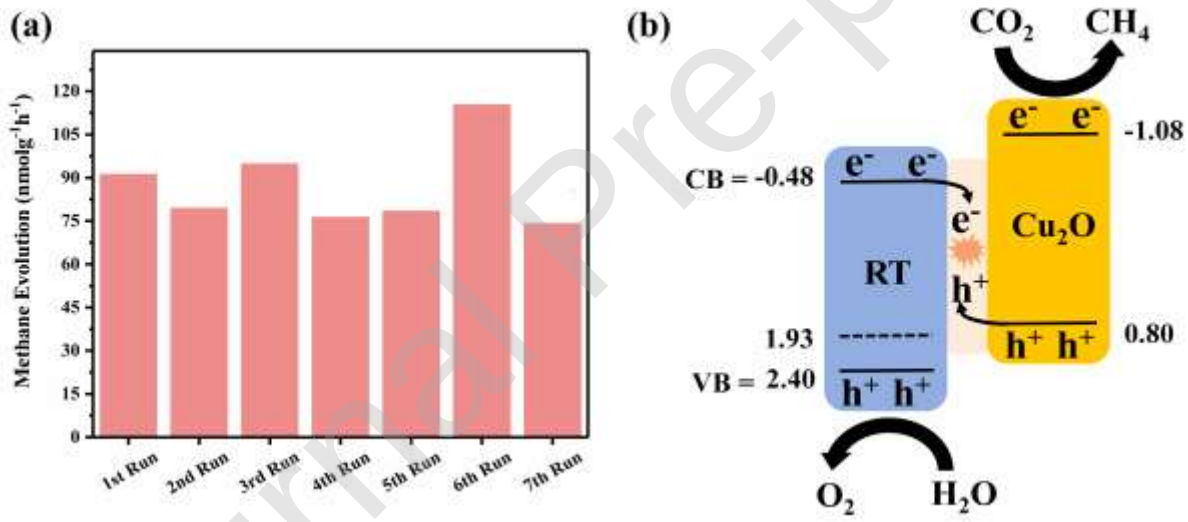

Fig. 7. (a) CH_4 evolution rate over seven sequential 6 h tests of a typical RT-$Cu_{0.75}$ sample, (b) energy band alignment (in V vs NHE at pH = 7), charge transfer and reaction mechanism for the described RT-Cu_2O Z-scheme showing $CO_2 + H_2O$ to CH_4 transformation.

Photocatalytic CO_2 reduction is challenging because it requires a semiconductor with highly negative conduction band ($CO_2 + e^- \rightarrow CO_2^{\bullet-}$ E°_{redox} = -1.90 V), which none of the photocatalysts possesses [3]. However, this can readily proceed when CO_2 is adsorbed upon the

surface of a V_o accompanying a Ti^{3+} state [47]. With adsorption the linear geometry of CO_2 is bent by which its LUMO level is decreased, thus the arduous first electron transfer which is considered as rate limiting step becomes feasible [5,66]. We propose such CO_2 activation upon the RT surface, after which it reduces to intermediate CO, Eq. (1) [65]. Such activation and subsequent conversion of CO_2 to CO, even under dark is well reported for synergistic effects of reduced titania and Cu [5]. Further, control test for P25-$Cu_{0.75}$, with approximately 5-fold less yield than RT-$Cu_{0.75}$ validates the efficacy of such activation by reduced titania, Fig. S8. Proceeding ahead, this CO readily anchors to Cu_2O through Cu^{1+}-CO interaction which allows only small amount to evade, Fig. 8a [5,67]. The affinity of the Cu^{1+} for CO, well reported in literature, helps to stabilize CO over the surface of Cu_2O as a consequence sustained supply of H^+ and electrons from CB of Cu_2O enable the formation of CH_4 preceded by the intermediate methyl radical ($\bullet CH_3$), Eq. (2-3) [5,68]. This route to CH_4 formation is confirmed by the appearance of IR bands of methyl radicals in contrast to fresh sample, Fig. 8b. These bands at 2925 and 2967 cm^{-1} are thought due to C-H stretching vibrations of the $\bullet CH_3$ radicals [69,70].

$$CO_2 + 2H^+ + 2e^- \rightarrow CO + H_2O \quad (1)$$

$$CO + 5H^+ + 5e^- \rightarrow \bullet CH_3 + H_2O \quad (2)$$

$$\bullet CH_3 + H^+ + e^- \rightarrow CH_4 \quad (3)$$

$$2H_2O + 2h^+ \rightarrow 2H^+ + 2\bullet OH \quad (4)$$

$$2H_2O + 2\bullet OH + 6h^+ \rightarrow 6H^+ + 2O_2 \quad (5)$$

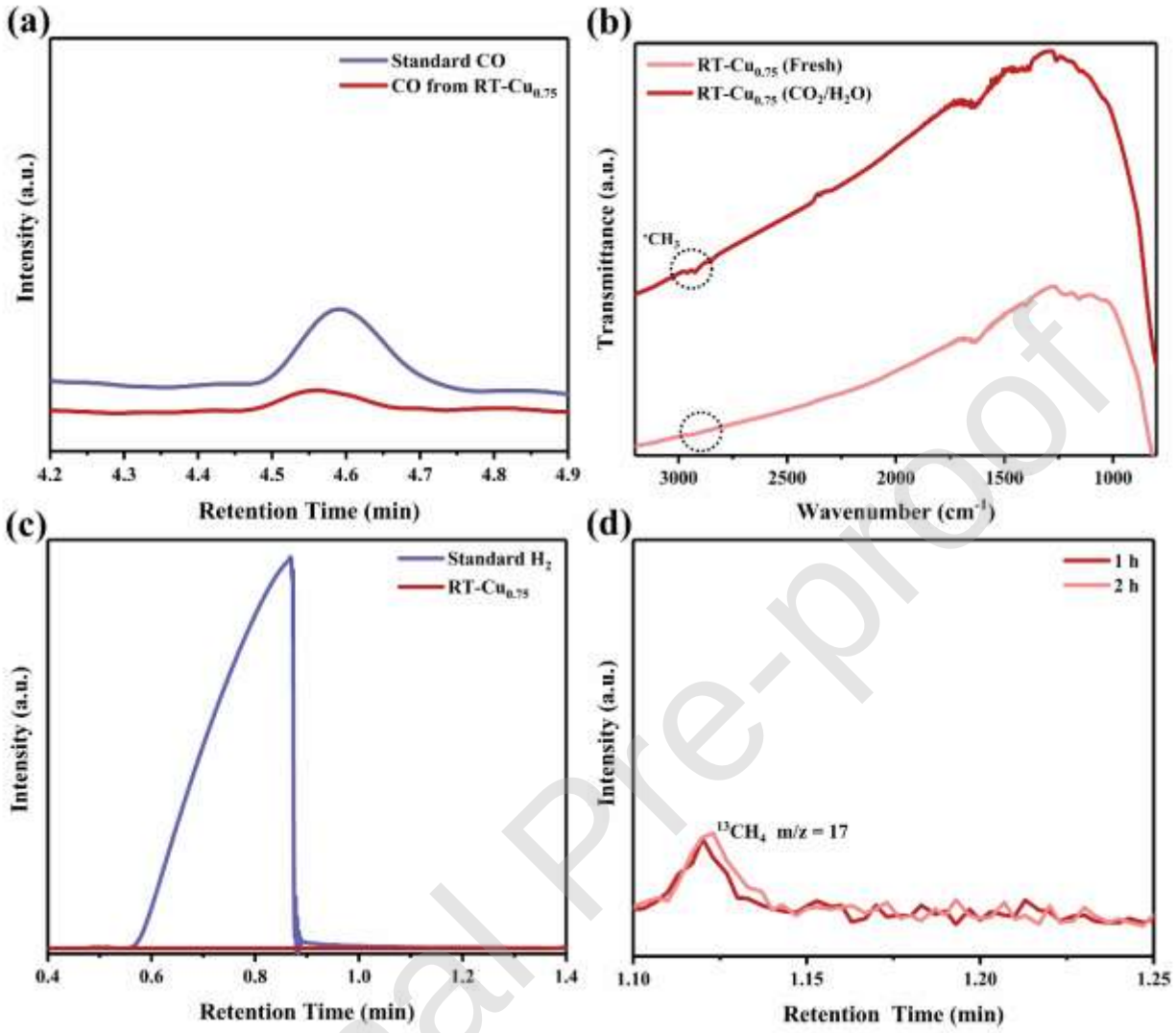

Fig. 8. Mechanistic study of the proposed reaction mechanism originating with a typical RT-$Cu_{0.75}$ sample, from (a) TCD chromatogram of CO; (b) FTIR spectra of •CH_3 radical; (c) TCD chromatogram of H_2; (d) GC-MS chromatogram of isotopic methane originating with $^{13}CO_2$.

The RT VB holes oxidize H_2O to H^+ and hydroxyl radicals (•OH), as confirmed by the coumarin dye test as shown in fig. S7 and Eq. (4). These generated •OH radicals further take part in water oxidation, Eq. (5), while H^+ in CO_2 reduction [71]. The absence of a H_2 peak, Fig. 8c, in GC-TCD chromatogram indicates that intermediate products of CO_2 reduction like CO are

stabilized enough to undergo proton coupled electron transport (PCET) for CH_4 formation which leave negligible H^+ ions for hydrogen formation [55].

Generation of $^{13}CH_4$ in the isotopic labeling experiment with $^{13}CO_2$ confirms the carbon origin is from CO_2, Fig. 8d. The control tests performed with photocatalyst under no illumination, and under illumination without a photocatalyst (blank reactor) showed no CH_4 formation, see Fig. S8. However, when the photocatalytic reaction proceeded in an inert He/H_2O atmosphere signature peak of CH_4 was observed and all the yields have been normalized against it [48].

4. Conclusions

A Z-scheme RT-Cu_2O heterojunction photocatalyst made of earth-plentiful materials for consistent conversion of CO_2 to fuel, notably CH_4, was constructed via low temperature thermochemical reduction of TiO_2 followed by photodeposition of Cu_2O. The photocatalytic reduction tests with optimal sample RT-$Cu_{0.75}$ exhibited excellent stability spanned over seven cycles while maintaining the activity for CH_4 generation. Synergistic integration of the Z-scheme structure, RT of which the V_o facilitate CO_2 activation and reduction, and Cu_2O with its highly reductive CB and excellent visible-light absorption properties resulted in a CO_2 conversion catalyst demonstrating excellent stability (42 h) without the need for scarce and expensive noble-metal co-catalysts.

Charge transfer studies confirm Z-scheme heterostructure formation, which prevents unwanted recombination of the strongly reductive Cu_2O CB electrons and RT oxidative VB holes. FTIR and GC-TCD/MS analysis was used to confirm the pathway by which CO_2 and water vapor

are converted to CH_4. That we are able to achieve consistent rates of CO_2 to CH_4 conversion and such extended operational stability with earth-plentiful compounds, by mass titanium comprising $\approx 0.57\%$ and copper $\approx 0.01\%$ of the earth's crust, suggests with improvement in yield scale-implementation of a commercial sunlight-based CO_2-fuel conversion industry is both viable and realistically achievable. We believe these results are not conclusive enough to estimate the peak activity of the photocatalyst, yield could be enhanced while optimizing the operational parameters like concentration/dilution of CO_2, operating pressure and CO_2 flow rate.

Contributions: S.-I. I. conceived and enabled the research, and contributed to writing the manuscript. S. A. contributed to material synthesis, analysis of experimental results, and writing the manuscript. J.L contributed to performing and interpreting the GC-MS results. H. K. assisted for hydrogen generation experiment and analysis as well. Y. H. helped to detect carbon monoxide. A. R helped to interpret the results and writing the manuscript. J. W. J. and C. H. C. analyzed the samples for time resolved PL.

Funding: The authors thankfully acknowledge the support of the Ministry of Science and ICT (2017R1E1A1A01074890 and 2017M2A2A6A01070912). This research was also supported by the Technology Development Program to Solve Climate Changes of the National Research Foundation (NRF) funded by the Ministry of Science and ICT (2015M1A2A2074670) and by Flux Photon Corporation.

Conflicts of Interest: The authors declare no conflict of interest.

Declaration of Interest Statement

The authors declare that they have no known competing financial interests or personal relationships that could have appeared to influence the work reported in this paper

References

[1] T.F. Stocker, A. Schmittner, Influence of CO_2 emission rates on the stability of the thermohaline circulation, Nature. 388 (1997) 862.

[2] S.E. Schwartz, Uncertainty in climate sensitivity: causes, consequences, challenges, Energy Environ. Sci. 1 (2008) 430–453.

[3] S. Ali, A. Razzaq, S.-I. In, Development of graphene based photocatalysts for CO_2 reduction to C_1 chemicals: A brief overview, Catal. Today. 335 (2018) 39–54.

[4] C.B. Hiragond, H. Kim, J. Lee, S. Sorcar, C. Erkey, S.-I. In, Electrochemical CO_2 Reduction to CO Catalyzed by 2D Nanostructures, Catalysts. 10 (2020) 98.

[5] L. Liu, C. Zhao, Y. Li, Spontaneous dissociation of CO_2 to CO on defective surface of Cu(I)/TiO_{2-x} nanoparticles at room temperature, J. Phys. Chem. C. 116 (2012) 7904–7912.

[6] S. Chu, A. Majumdar, Opportunities and challenges for a sustainable energy future, Nature. 488 (2012) 294.

[7] Y. Qu, X. Duan, Progress, challenge and perspective of heterogeneous photocatalysts, Chem. Soc. Rev. 42 (2013) 2568–2580.

[8] C. Hiragond, S. Ali, S. Sorcar, S.-I. In, Hierarchical Nanostructured Photocatalysts for CO_2 Photoreduction, Catalysts. 9 (2019) 370.

[9] A. Razzaq, A. Sinhamahapatra, T.H. Kang, C.A. Grimes, J.S. Yu, S.-I. In, Efficient solar light photoreduction of CO_2 to hydrocarbon fuels via magnesiothermally reduced TiO_2 photocatalyst, Appl. Catal. B Environ. 215 (2017) 28–35.

[10] D. Ning, H. Wei, G. Ou, R. Zhang, H. Wu, Copper reduced defective TiO_2 nanoparticles with enhanced visible light photocatalytic activity, J. Am. Ceram. Soc. 101 (2018) 4857–4863.

[11] S. Sorcar, Y. Hwang, C.A. Grimes, S.-I. In, Highly enhanced and stable activity of defect-induced titania nanoparticles for solar light-driven CO_2 reduction into CH_4, Mater. Today. 20 (2017) 507–515.

[12] S.G. Ullattil, S.B. Narendranath, S.C. Pillai, P. Periyat, Black TiO_2 Nanomaterials: A Review of Recent Advances, Chem. Eng. J. 343 (2018) 708–736.

[13] L.-L. Tan, W.-J. Ong, S.-P. Chai, A.R. Mohamed, Noble metal modified reduced graphene oxide/TiO_2 ternary nanostructures for efficient visible-light-driven photoreduction of carbon dioxide into methane, Appl. Catal. B Environ. 166 (2015) 251–259.

[14] S. Sorcar, J. Thompson, Y. Hwang, Y.H. Park, T. Majima, C.A. Grimes, J.R. Durrant, S.-I. In, High-rate solar-light photoconversion of CO_2 to fuel: Controllable transformation from C_1 to C_2 products, Energy Environ. Sci. 11 (2018) 3183–3193.

[15] T. Wei, Y.N. Zhu, X. An, L.M. Liu, X. Cao, H. Liu, J. Qu, Defect Modulation of Z-Scheme TiO_2/Cu_2O Photocatalysts for Durable Water Splitting, ACS Catal. 9 (2019) 8346–8354.

[16] K.C. Christoforidis, P. Fornasiero, Photocatalysis for Hydrogen Production and CO_2 Reduction: The Case of Copper-Catalysts, ChemCatChem. 11 (2019) 368–382.

[17] L.-Y. Lin, Y. Nie, S. Kavadiya, T. Soundappan, P. Biswas, N-doped reduced graphene oxide promoted nano TiO_2 as a bifunctional adsorbent/photocatalyst for CO_2 photoreduction: Effect of N species, Chem. Eng. J. 316 (2017) 449–460.

[18] O.K. Varghese, M. Paulose, T.J. LaTempa, C.A. Grimes, High-rate solar photocatalytic conversion of CO_2 and water vapor to hydrocarbon fuels, Nano Lett. 9 (2009) 731–737.

[19] L. Yu, X. Ba, M. Qiu, Y. Li, L. Shuai, W. Zhang, Z. Ren, Y. Yu, Visible-light driven CO_2 reduction coupled with water oxidation on Cl-doped Cu_2O nanorods, Nano Energy. 60 (2019) 576–582.

[20] P.V. Danckwerts, Z-Scheme Photocatalytic Systems for Carbon Dioxide Reduction: Where Are We Now?, Chem. Eng. Sci. 17 (1962) 955.

[21] M.E. Aguirre, R. Zhou, A.J. Eugene, M.I. Guzman, M.A. Grela, Cu_2O/TiO_2 heterostructures for CO_2 reduction through a direct Z-scheme: Protecting Cu_2O from photocorrosion, Appl. Catal. B Environ. 217 (2017) 485–493.

[22] J. Xing, Z.P. Chen, F.Y. Xiao, X.Y. Ma, C.Z. Wen, Z. Li, H.G. Yang, Cu-Cu_2O-TiO_2 nanojunction systems with an unusual electron-hole transportation pathway and enhanced photocatalytic properties, Chem. - An Asian J. 8 (2013) 1265–1270.

[23] J. Low, C. Jiang, B. Cheng, S. Wageh, A.A. Al-Ghamdi, J. Yu, A Review of Direct Z-Scheme Photocatalysts, Small Methods. 1 (2017) 1700080.

[24] P. Zhou, J. Yu, M. Jaroniec, All-solid-state Z-scheme photocatalytic systems, Adv. Mater. 26 (2014) 4920–4935.

[25] Q. Yuan, D. Liu, N. Zhang, W. Ye, H. Ju, L. Shi, R. Long, J. Zhu, Y. Xiong, Noble-Metal-

Free Janus-like Structures by Cation Exchange for Z-Scheme Photocatalytic Water Splitting under Broadband Light Irradiation, Angew. Chemie Int. Ed. 129 (2017) 4270–4274.

[26] Y. Liu, B. Zhang, L. Luo, X. Chen, Z. Wang, E. Wu, D. Su, W. Huang, TiO_2/Cu_2O core/ultrathin shell nanorods as efficient and stable photocatalysts for water reduction, Angew. Chemie Int. Ed. 54 (2015) 15260–15265.

[27] Q. Xu, L. Zhang, J. Yu, S. Wageh, A.A. Al-Ghamdi, M. Jaroniec, Direct Z-scheme photocatalysts: Principles, synthesis, and applications, Mater. Today. 21 (2018) 1042–1063.

[28] Y. Lou, Y. Zhang, L. Cheng, J. Chen, Y. Zhao, A stable plasmonic $Cu@Cu_2O/ZnO$ heterojunction for enhanced photocatalytic hydrogen generation, ChemSusChem. 11 (2018) 1505–1511.

[29] S.C. Wu, C.S. Tan, M.H. Huang, Strong Facet Effects on Interfacial Charge Transfer Revealed through the Examination of Photocatalytic Activities of Various Cu_2O–ZnO Heterostructures, Adv. Funct. Mater. 27 (2017) 1604635.

[30] S. Ali, M.C. Flores, A. Razzaq, S. Sorcar, C.B. Hiragond, H.R. Kim, Y.H. Park, Y. Hwang, H.S. Kim, H. Kim, S.-I. In, Gas Phase Photocatalytic CO_2 Reduction,"A Brief Overview for Benchmarking," Catalysts. 9 (2019) 727.

[31] G. Zhu, C. Yang, F. Huang, Z. Wang, H. Yin, J. Lin, Z. Liu, W. Zhao, T. Lin, X. Lü, Black brookite titania with high solar absorption and excellent photocatalytic performance, J. Mater. Chem. A. 1 (2013) 9650.

[32] Y. Li, W.N. Wang, Z. Zhan, M.H. Woo, C.Y. Wu, P. Biswas, Photocatalytic reduction of CO_2 with H_2O on mesoporous silica supported Cu/TiO_2 catalysts, Appl. Catal. B Environ.

100 (2010) 386–392.

[33] X. Qian, H. Han, Y. Chen, Y. Yuan, Sol–gel solvothermal route to synthesize anatase/brookite/rutile TiO_2 nanocomposites with highly photocatalytic activity, J. Sol-Gel Sci. Technol. 85 (2018) 394–401.

[34] Y. Yan, M. Han, A. Konkin, T. Koppe, D. Wang, T. Andreu, G. Chen, U. Vetter, J.R. Morante, P. Schaaf, Slightly hydrogenated TiO_2 with enhanced photocatalytic performance, J. Mater. Chem. A. 2 (2014) 12708–12716.

[35] L. Zou, J. Li, D. Zakharov, E.A. Stach, G. Zhou, In situ atomic-scale imaging of the metal/oxide interfacial transformation, Nat. Commun. 8 (2017) 1–8.

[36] Z. Tan, T. Peng, X. Tan, W. Wang, X. Wang, Z. Yang, H. Ning, Q. Zhao, M. Wu, Controllable synthesis of leaf- like CuO nanosheets for selective CO_2 electroreduction to ethylene, ChemElectroChem. 7 (2020) 2020-2025.

[37] X. Qiu, M. Miyauchi, K. Sunada, M. Minoshima, M. Liu, Y. Lu, D. Li, Y. Shimodaira, Y. Hosogi, Y. Kuroda, K. Hashimoto, Hybrid Cu_xO/TiO_2 nanocomposites as risk-reduction materials in indoor environments, ACS Nano. 6 (2012) 1609–1618.

[38] J. Yu, J. Ran, Facile preparation and enhanced photocatalytic H_2-production activity of Cu $(OH)_2$ cluster modified TiO_2, Energy Environ. Sci. 4 (2011) 1364–1371.

[39] K. Wenderich, G. Mul, Methods, Mechanism, and Applications of Photodeposition in Photocatalysis: A Review, Chem. Rev. 116 (2016) 14587–14619.

[40] Q. Kang, J. Cao, Y. Zhang, L. Liu, H. Xu, J. Ye, Reduced TiO_2 nanotube arrays for photoelectrochemical water splitting, J. Mater. Chem. A. 1 (2013) 5766–5774.

[41] X. Pan, M.Q. Yang, X. Fu, N. Zhang, Y.J. Xu, Defective TiO_2 with oxygen vacancies: Synthesis, properties and photocatalytic applications, Nanoscale. 5 (2013) 3601–3614.

[42] J.D. Schneider, B.A. Smith, G.A. Williams, D.R. Powell, F. Perez, G.T. Rowe, L. Yang, Synthesis and Characterization of Cu(II) and Mixed-Valence Cu(I)Cu(II) Clusters Supported by Pyridylamide Ligands, Inorg. Chem. 59 (2020) 5433-5446.

[43] S. Wu, G. Fu, W. Lv, J. Wei, W. Chen, H. Yi, M. Gu, X. Bai, L. Zhu, C. Tan, Y. Liang, G. Zhu, J. He, X. Wang, K.H.L. Zhang, J. Xiong, W. He, A Single-Step Hydrothermal Route to 3D Hierarchical Cu_2O/CuO/rGO Nanosheets as High-Performance Anode of Lithium-Ion Batteries, Small. 14 (2018) 1–8.

[44] M. Yin, C.K. Wu, Y. Lou, C. Burda, J.T. Koberstein, Y. Zhu, S. O'Brien, Copper oxide nanocrystals, J. Am. Chem. Soc. 127 (2005) 9506–9511.

[45] T. Arai, M. Horiguchi, M. Yanagida, T. Gunji, H. Sugihara, K. Sayama, Reaction mechanism and activity of WO_3-catalyzed photodegradation of organic substances promoted by a CuO cocatalyst, J. Phys. Chem. C. 113 (2009) 6602–6609.

[46] S.M. Pawar, J. Kim, A.I. Inamdar, H. Woo, Y. Jo, B.S. Pawar, S. Cho, H. Kim, H. Im, Multi-functional reactively-sputtered copper oxide electrodes for supercapacitor and electro-catalyst in direct methanol fuel cell applications, Sci. Rep. 6 (2016) 1–9.

[47] K. Lalitha, G. Sadanandam, V.D. Kumari, M. Subrahmanyam, B. Sreedhar, N.Y. Hebalkar, Highly stabilized and finely dispersed Cu_2O/TiO_2: A promising visible sensitive photocatalyst for continuous production of hydrogen from glycerol:water mixtures, J. Phys. Chem. C. 114 (2010) 22181–22189.

[48] G.W. Busser, B. Mei, A. Pougin, J. Strunk, R. Gutkowski, W. Schuhmann, M. Willinger, R. Schlögl, M. Muhler, Photodeposition of Copper and Chromia on Gallium Oxide: The Role of Co- Catalysts in Photocatalytic Water Splitting, ChemSusChem. 7 (2014) 1030–1034.

[49] L. Yuan, S.F. Hung, Z.R. Tang, H.M. Chen, Y. Xiong, Y.J. Xu, Dynamic Evolution of Atomically Dispersed Cu Species for CO_2 Photoreduction to Solar Fuels, ACS Catal. 9 (2019) 4824–4833.

[50] J. Lee, D.C. Sorescu, X. Deng, Electron-induced dissociation of CO_2 on TiO_2(110), J. Am. Chem. Soc. 133 (2011) 10066–10069.

[51] J. Jin, J. Yu, D. Guo, C. Cui, W. Ho, A Hierarchical Z- Scheme CdS–WO_3 Photocatalyst with Enhanced CO_2 Reduction Activity, Small. 11 (2015) 5262–5271.

[52] J. Bian, Y. Qu, X. Zhang, N. Sun, D. Tang, L. Jing, Dimension-matched plasmonic Au/TiO_2/$BiVO_4$ nanocomposites as efficient wide-visible-light photocatalysts to convert CO_2 and mechanistic insights, J. Mater. Chem. A. 6 (2018) 11838–11845.

[53] R. Fu, S. Gao, H. Xu, Q. Wang, Z. Wang, B. Huang, Y. Dai, Fabrication of Ti^{3+} self-doped TiO_2(A) nanoparticle/TiO_2(R) nanorod heterojunctions with enhanced visible-light-driven photocatalytic properties, RSC Adv. 4 (2014) 37061–37069.

[54] X. Chen, L. Liu, Y.Y. Peter, S.S. Mao, Increasing solar absorption for photocatalysis with black hydrogenated titanium dioxide nanocrystals, Science (80-.). 331 (2011) 746–750.

[55] Z. Xiong, Z. Lei, C.C. Kuang, X. Chen, B. Gong, Y. Zhao, J. Zhang, C. Zheng, J.C.S. Wu, Selective photocatalytic reduction of CO_2 into CH_4 over Pt-Cu_2O TiO_2 nanocrystals: The

interaction between Pt and Cu_2O cocatalysts, Appl. Catal. B Environ. 202 (2017) 695–703.

[56] Y. You, W. Tian, L. Min, F. Cao, K. Deng, L. Li, TiO_2 /WO_3 Bilayer as Electron Transport Layer for Efficient Planar Perovskite Solar Cell with Efficiency Exceeding 20%, Adv. Mater. Interfaces. 7 (2019) 1901406.

[57] X. Shi, Y. Ding, S. Zhou, B. Zhang, M. Cai, J. Yao, L. Hu, J. Wu, S. Dai, M.K. Nazeeruddin, Enhanced Interfacial Binding and Electron Extraction Using Boron-Doped TiO_2 for Highly Efficient Hysteresis-Free Perovskite Solar Cells, Adv. Sci. 6 (2019) 1901213.

[58] Y.P. Xie, Y. Yang, G. Wang, G. Liu, Oxygen vacancies promoted interfacial charge carrier transfer of CdS/ZnO heterostructure for photocatalytic hydrogen generation, J. Colloid Interface Sci. 503 (2017) 198–204.

[59] H.J. Yun, H. Lee, N.D. Kim, D.M. Lee, S. Yu, J. Yi, A combination of two visible-light responsive photocatalysts for achieving the Z-scheme in the solid state, ACS Nano. 5 (2011) 4084–4090.

[60] M. Dilla, R. Schlögl, J. Strunk, Photocatalytic CO_2 Reduction Under Continuous Flow High-Purity Conditions: Quantitative Evaluation of CH_4 Formation in the Steady-State, ChemCatChem. 9 (2017) 696–704.

[61] G.W. Busser, B. Mei, M. Muhler, Optimizing the Deposition of Hydrogen Evolution Sites on Suspended Semiconductor Particles using On- Line Photocatalytic Reforming of Aqueous Methanol Solutions, ChemSusChem. 5 (2012) 2200–2206.

[62] W. Kim, T. Seok, W. Choi, Nafion layer-enhanced photosynthetic conversion of CO_2 into hydrocarbons on TiO_2 nanoparticles, Energy Environ. Sci. 5 (2012) 6066–6070.

[63] M.A.L.R.M. Cortes, J.W.J. Hamilton, P.K. Sharma, A. Brown, M. Nolan, K.A. Gray, J.A. Byrne, Formal quantum efficiencies for the photocatalytic reduction of CO_2 in a gas phase batch reactor, Catal. Today. 326 (2019) 75–81.

[64] S. Sorcar, Y. Hwang, J. Lee, H. Kim, K.M. Grimes, C.A. Grimes, J.-W. Jung, C.-H. Cho, T. Majima, M.R. Hoffmann, S.-I. In, CO_2, water, and sunlight to hydrocarbon fuels: a sustained sunlight to fuel (Joule-to-Joule) photoconversion efficiency of 1%, Energy Environ. Sci. 12 (2019) 2685-2696.

[65] S. Zhu, S. Liang, Y. Tong, X. An, J. Long, X. Fu, X. Wang, Photocatalytic reduction of CO_2 with H_2O to CH_4 on Cu(i) supported TiO_2 nanosheets with defective {001} facets, Phys. Chem. Chem. Phys. 17 (2015) 9761–9770.

[66] Y. Chen, C.W. Li, M.W. Kanan, Aqueous CO_2 reduction at very low overpotential on oxide-derived au nanoparticles, J. Am. Chem. Soc. 134 (2012) 19969–19972.

[67] L. Liu, F. Gao, H. Zhao, Y. Li, Tailoring Cu valence and oxygen vacancy in Cu/TiO_2 catalysts for enhanced CO_2 photoreduction efficiency, Appl. Catal. B Environ. 134 (2013) 349–358.

[68] Y. Ji, Y. Luo, New mechanism for photocatalytic reduction of CO_2 on the anatase TiO_2 (101) surface: The essential role of oxygen vacancy, J. Am. Chem. Soc. 138 (2016) 15896–15902.

[69] A.S. Poyraz, S. Biswas, H.C. Genuino, S. Dharmarathna, C. Kuo, S.L. Suib, Bimodification of Mesoporous Silicon Oxide by Coupled “In Situ Oxidation at the Interface and Ion Exchange” and its Catalytic Activity in the Gas- Phase Toluene Oxidation, ChemCatChem.

5 (2013) 920–930.

[70] Z. Tan, W. Zhang, Z. Zhang, D. Qian, Y. Huang, J. Hou, Y. Li, High- Performance Inverted Polymer Solar Cells with Solution- Processed Titanium Chelate as Electron- Collecting Layer on ITO Electrode, Adv. Mater. 24 (2012) 1476–1481.

[71] M. Tahir, N.A.S. Amin, Indium-doped TiO_2 nanoparticles for photocatalytic CO_2 reduction with H_2O vapors to CH_4, Appl. Catal. B Environ. 162 (2015) 98–109.